ARTICLE

Phosphorescent Cationic Iridium(III) Complexes with 1,3,4-Oxadiazole Cyclometalating Ligands: Solvent-Dependent Excited-State Dynamics

Zhuoran Kuang[a,b], Xian Wang[a,b], Zhen Wang[c], Guiying He[a,b], Qianjin Guo[a], Lei He[c*], Andong Xia[a,b*]

a. Beijing National Laboratory for Molecular Sciences (BNLMS), Key Laboratory of Photochemistry, Institute of Chemistry, Chinese Academy of Sciences, Beijing 100190, China
b. University of Chinese Academy of Sciences, Beijing 100049, China
c. College of Chemistry and Chemical Engineering, Central South University, Changsha 410083, China

(Dated: Received on March 29, 2017; Accepted on May 16, 2017)

To elucidate the nature of low-lying triplet states and the effect of ligand modifications on the excited-state properties of functional cationic iridium complexes, the solvent-dependent excited-state dynamics of two phosphorescent cationic iridium(III) complexes, namely [Ir(dph-oxd)$_2$(bpy)]PF$_6$ (**1**) and [Ir(dph-oxd)$_2$(pzpy)]PF$_6$ (**2**), were investigated by femtosecond and nanosecond transient absorption spectroscopy. Upon photoexcitation to the metal-to-ligand charge-transfer (MLCT) states, the excited-state dynamics shows a rapid process (τ=0.7−3 ps) for the formation of solvent stabilized ^{3}MLCT states, which significantly depends on the solvent polarity for both **1** and **2**. Sequentially, a relatively slow process assigned to the vibrational cooling/geometrical relaxation and a long-lived phosphorescent emissive state is identified. Due to the different excited-state electronic structures regulated by ancillary ligands, the solvation-induced stabilization of the ^{3}MLCT state in **1** is faster than that in **2**. The present results provide a better sight of excited-state relaxation dynamics of ligand-related iridium(III) complexes and solvation effects on triplet manifolds.

Key words: Iridium complex, Phosphorescence, Metal-to-ligand charge transfer, Transient absorption, Solvation

I. INTRODUCTION

In recent years, the study of phosphorescent cyclometalated iridium(III) complexes have attracted enormous attention from academic to industrial communities in the development of phosphorescent organic light-emitting diodes (PHOLEDs) due to their potential applications in full-color displays and energy-saving solid-state lightings [1–3]. In addition to their superior photoluminescence and electroluminescence properties, cyclometalated iridium(III) complexes have been found to act as long-lived triplet photosensitizers with outstanding performances, which extensively expand applications in triplet-triplet annihilation (TTA) [4, 5], dye-sensitized solar cells (DSSCs) [6], sensitization of singlet oxygen [7], and photocatalytic water splitting [8].

As a third-row transition metal cation with an electron configuration of 5d^6, iridium(III) is capable of forming cyclometalated cationic complexes, referred as [Ir(C^N)$_2$(N^N)]$^+$A$^-$, with the cyclometalating ligands (C^N), the ancillary ligand (N^N) and the counter anion (A$^-$) [9, 10]. For this type of iridium(III) complexes, the frontier molecular orbitals are delocalized over the entire molecule with remarkable charge-transfer characteristics. The highest occupied molecular orbitals (HOMOs) are usually delocalized on the d orbitals of iridium(III) and π orbitals of cyclometalating ligands, while the lowest unoccupied molecular orbitals (LUMOs) have dominant contributions from π^* orbitals of ancillary ligands [11, 12]. The HOMO and LUMO energies can be modified by respectively alternating the C^N and N^N ligands, and then the characteristics of excited-states and the photochemical performances are artificially controlled [12]. The photoexcitation mainly promotes three electronic transitions, which are characterized as metal-to-ligand charge-transfer (MLCT), ligand-to-ligand charge-transfer (LLCT) and ligand-centered (LC) transitions [12]. Importantly, the excited singlet states undergo very rapid intersystem crossing (ISC), resulting in the excited triplet manifold population, as a consequence of a high spin-orbit coupling (SOC) constant (3909 cm^{-1}) compared to some well-known octahedral coordination complexes of Fe (431 cm^{-1}), Ru (1042 cm^{-1}), Os (3381 cm^{-1}), which is in direct proportion to the biquadrate of the atomic number [13, 14]. Thus, the strong SOC in iridium(III) complexes achieves the internal quantum efficiency ap-

*Authors to whom correspondence should be addressed. E-mail: andong@iccas.ac.cn, helei06@csu.edu.cn

proaching ∼100% [1, 3, 15–17]. The kinetic of ISC process of some iridium(III) complexes has been investigated using femtosecond photoluminescence spectroscopy, which reveals that the ISC has a time scale down to or even less than 100 fs [18, 19]. The rate of the ultrafast ISC is equivalent to that of internal conversion (IC), indicating that the spin-flipped transition is not a rate-determining process [20]. Furthermore, the spin-forbidden nature of the transitions from the triplet manifold to the ground state are moderately removed by the strong SOC, inducing the intense room-temperature phosphorescence [21].

For iridium(III) complexes with efficient ISC, the lowest triplet state emitting phosphorescence, according to Kasha's rule, is either a ^{3}MLCT or a ^{3}LC state [22]. The relaxation processes of excited-states, which are accompanied by the intramolecular charge-transfer (ICT), are significantly affected by solvation effects [23–25]. After the redistribution of charge density on solute molecules induced by the photoexcitation, the surrounding solvent electric dipoles rearrange around the excited solute molecules, which affects the excited-state relaxation processes [26, 27]. By investigating the solute-solvent interaction, especially the dynamics response, the sequential evolution among the excited-state manifold could be resolved clearly with the aid of ultrafast pump-probe transient absorption techniques [28]. So far, for a wide variety of ligand-dependent functional transition metal complexes with efficient ISC, excited-state deactivation processes from Franck-Condon excitations to emissive triplet states, which are accompanied with changes of electronic configuration, solvent response, geometric structure and thermal equilibrium, still remain a subject of debate and confusion regarding the photophysical nature and characteristic time scale [29–33].

Currently, much attention concentrates on the structure-property relationship of heavy metal complexes to design, modify and optimize their photoluminescence and photosensitization properties, where ligands are the key factors to control the relative energies of frontier orbitals and excited-state relaxation dynamics [34]. We recently reported the synthesis of [Ir(dph-oxd)$_2$(bpy)]PF$_6$ (**1**) and [Ir(dph-oxd)$_2$(pzpy)]PF$_6$ (**2**) (their molecular structures are shown in Scheme 1), with the cyclometalating ligand of 2,5-diphenyl-1,3,4-oxadiazole (dph-oxd) and the ancillary ligands of 2,2′-bipyridine (bpy) and 2-(1H-pyrazol-1-yl)pyridine (pzpy), respectively [10]. Due to the stabilization of HOMO levels induced by the electron-deficient oxadiazole heterocycle in dph-oxd, complexes **1** and **2** have wide energy gaps (∼2.8−3.5 eV) and efficient blue-green (480−580 nm) phosphorescent emissions [10, 34]. In addition, complex **2** in which the electron-rich pzpy substitutes the bpy, presents a largely enhanced LUMO level relative to complex **1**. Although their basic photophysical and electrochemical properties have been discussed, the excited-state dynamic processes of complexes **1** and **2** are unclear and need to be investigated. Above all, elucidating the nature of their low-lying triplet states is of great significant to understand the origin of phosphorescence and further reveal the ligand-related excited-state behaviours in iridium(III) complexes.

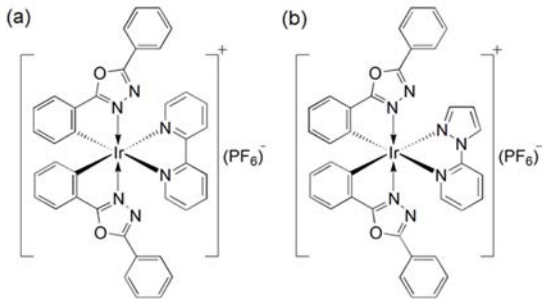

Scheme 1 Molecular structures of (a) [Ir(dph-oxd)$_2$(bpy)]PF$_6$ (**1**) and (b) [Ir(dph-oxd)$_2$(pzpy)]PF$_6$ (**2**).

In the present work, to reveal and understand the photoluminescence properties and solvent-dependent excited states dynamics of iridium(III) complexes in the excited triplet manifold, ultrafast transient absorption spectroscopy is employed for complexes **1** and **2** in solutions. Three aprotic solvents (chloroform, tetrahydrofuran and acetonitrile) with different polarities are used to monitor the excited-state relaxation dynamics and the electronic state evolutions. Focusing on the solvation response induced by dipole-dipole interaction, the temporal electric dipole change of excited complexes could be identified. With steady-state spectral measurements and theoretical calculations, the ICT characteristic in excited states of both complexes have been intensively studied. The femtosecond transient absorption spectroscopy upon the MLCT state excitation shows a rapid process attributed to the generation of solvent stabilized ^{3}MLCT state, which is relevant to the solvent polarity. In addition, the vibrational cooling/geometrical relaxations and long-lived phosphorescent emission states are also identified.

II. EXPERIMENTS

A. Materials

The synthesis of [Ir(dph-oxd)$_2$(bpy)]PF$_6$ (complex **1**) and [Ir(dph-oxd)$_2$(pzpy)]PF$_6$ (complex **2**) has been described in detail elsewhere [10]. Briefly, for the synthesis of complex **1**, [Ir(dph-oxd)$_2$Cl]$_2$ reacted with bpy in CH_2Cl_2/CH_3OH. After evaporation, and the residual was dissolved in deionized water and KPF_6 was added to the solution to form [Ir(dph-oxd)$_2$(bpy)]$^+$. The synthesis of complex **2** was similar to that for complex **1**, except that pzpy substituted bpy. Purified complexes were dissolved in solvents (*i.e.* dichloromethane, acetonitrile, tetrahydrofuran) for spectroscopic measurements. All solvents involved were spectroscopic grade

DOI:10.1063/1674-0068/30/cjcp1703058

and used as received.

B. Quantum chemical calculations

On the basis of density-functional theory (DFT), quantum-chemical calculations were performed to obtain the optimized geometries and electronic structures for complex **1** and complex **2**. The method using B3LYP with basis sets of 6-31G(d,p) for C, H, N and O, and LANL2DZ for Ir was employed to fully optimize the ground-state geometries without any symmetry constraints. The vertical excitation energies of low-lying excited-states were calculated on the optimized ground-state geometries with the time-dependent DFT (TD-DFT) approach. Considering the solvent effects, self-consistent reaction field (SCRF) theory adopting the polarized continuum model (PCM) was applied. All calculations were carried out for isolated molecules and conducted with the Gaussian 09 software package [35].

C. Steady state and transient absorption spectral measurements

The steady-state ultraviolet-visible absorption and photoluminescence spectra were measured on a U3010 (Hitachi) spectrometer and an F4600 (Hitachi) fluorescence spectrometer, respectively. The nanosecond transient absorption measurements were performed using a nanosecond flash photolysis spectrometer (LP920, Edinburgh Instruments), excited by a Nd:YAG laser (Quanta-Ray, Spectra-Physics) at 355 nm with the FWHM of 8 ns. The femtosecond transient absorption spectra with ∼100 fs time-resolution were measured on a home-built femtosecond broadband pump-probe setup, which has been described elsewhere [36, 37]. Briefly, a pulse with 400 nm, 50 fs, 90 nJ and 1 kHz from a regenerative amplified femtosecond laser acts as the pump beam focused (spot size is about 130 μm) on the sample. A white light supercontinuum (420−780 nm) generated by a water cell acts as a probe beam after an optical delay up to 1 ns. The thickness of flowing sample cells is 1 mm for transient measurements. For isotropic measurements, the angle of pump and probe beam polarization was set to the magic angle (54.7°). Before the data analysis, the chirp correction has been conducted to calibrate the spectral chirp caused by group velocity delay dispersion of the supercontinuum probe beam in femtosecond transient absorption spectra. The time evolution differential absorbance $\Delta A(t,\lambda)$ was analyzed by singular value decomposition (SVD) and global analysis using Glotaran and TIMP software package [38, 39]. $\Delta A(t,\lambda)$ is a superposition of several principal spectral components $\varepsilon_i(\lambda)$ weighed by their concentrations $c_i(t)$ [38, 40]:

$$\Delta A\,(t,\lambda) = \sum_{i=1}^{n} c_i\,(t)\varepsilon_i\,(\lambda) \qquad (1)$$

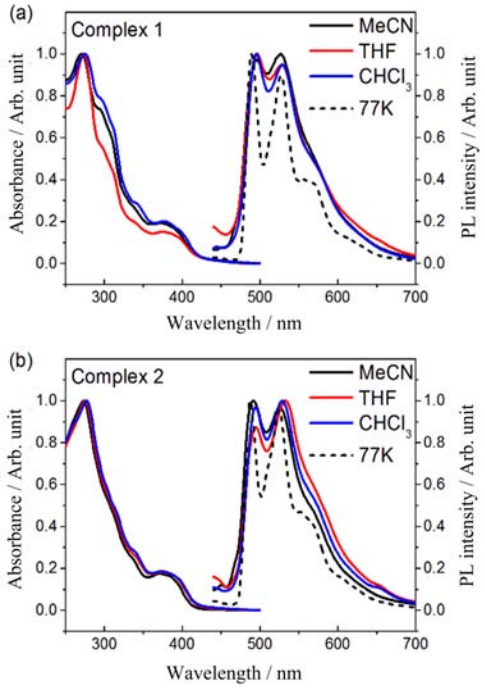

FIG. 1 Normalized steady-state absorption and PL spectra of (a) complex **1** and (b) complex **2**. The PL spectra were measured with excitation at 400 nm. The PL spectra at 77 K were measured in MeCN glass.

III. RESULTS AND DISCUSSION

A. Steady state spectra

The normalized absorption and luminescence spectra of complexes **1** and **2** in acetonitrile (MeCN), tetrahydrofuran (THF) and chloroform ($CHCl_3$) at 298 and 77 K (in MeCN glass) are shown in FIG. 1. The profiles of the absorption spectra are similar for both complexes **1** and **2** in different polar solvents. The intense absorption bands below 350 nm in ultraviolet region are assigned to the spin-allowed $^1\pi$-π^* transitions of the cyclometalating ligands or ancillary ligands, forming the intramolecular ^{1}LC states [41]. These bands extending from 350 nm to 450 nm show relatively lower absorption features, which are ascribed to spin-allowed or forbidden ^{1}MLCT/^{3}MLCT states, ^{1}LLCT/^{3}LLCT states and weak ^{3}LC transitions [41]. Here, the spin-forbidden transitions are moderately released by the strong SOC endowed by the heavy atom effect, which brings a certain extent of absorption and efficient phosphorescence emission at room-temperature [14].

Both complexes **1** and **2** emit green phosphorescence at 298 and 77 K with structured emission spectra. Detailed emission characteristics are displayed in Table I. At 298 K, their emission peaks show slight red-shifts relative to those at 77 K. The structured phosphorescence emission curves with weak solvatochromism and rigidochromism indicate that $^3\pi$-π^* character dominates the lowest emissive triplet states [12]. The sim-

DOI:10.1063/1674-0068/30/cjcp1703058

TABLE I Emission characteristics of complexes **1** and **2** in solutions. ε is the dielectric constant of the solvent [44].

	Solvent	ε	Quantum yield	Emission λ_{peak}/nm	
				77 K	298 K
1	MeCN	35.94	0.31±0.02	490, 527, 568	496, 527
2			0.33±0.02	488, 524, 561	492, 525
1	THF	7.58	0.48±0.02	495, 530, 564	497, 529
2			0.30±0.02	494, 528, 562	495, 532
1	$CHCl_3$	4.81	0.68±0.02	491, 528, 563	495, 529
2			0.48±0.02	489, 526, 561	494, 529

ilar emission curves of complexes **1** and **2** indicate that their emission properties are dominated by the cyclometalating ligands of dph-oxd, which bears an electron-withdrawing group, forming the emissive dph-oxd-centered ($^3\pi$-π^*) states [10, 42, 43].

For general iridium(III) complexes, on account of the spin-flip exchange energy, the energetic order of these transition is ^{1}LC>^{1}MLCT>^{3}MLCT>^{3}LC [12]. The lowest triplet states, which emit efficient phosphorescence, have a hybrid feature of ^{3}MLCT and ^{3}LC. It is found that the luminescence quantum yields of both complexes **1** and **2** are remarkably solvent-dependent, as shown in Table I. For complex **1**, the quantum yields are measured to be ∼0.31 in MeCN (ε=35.94), ∼0.48 in THF (ε=7.58) and ∼0.68 in $CHCl_3$ (ε=4.81), which are similar to those for complex **2**. For complexes **1** and **2**, strong non-radiative transitions induced by solvation occur before reaching the lowest emissive state, leading to the quenching of luminescence in highly polar solvents [45]. In this case, the ^{3}MLCT states, which are closely associated with solvation processes, are located at higher energy than the emissive ^{3}LC states.

In our previous work, the emission spectrum of complex **1** exhibited an obvious red-shift and a structure-loss when increasing its doping concentration in the poly(methyl methacrylate) matrix, whereas complex **2** always exhibited structured emission spectra with negligible red-shifts. Also, a reversible piezochromic behavior was observed for complex **1** [10]. These experimental results indicate that for complex **1**, the LC $^3\pi$-π^* and ^{3}MLCT/^{3}LLCT triplet states are close-lying in energy and account for the final emitting states [10, 46–50]. In contrast, the lowest triplet states of complex **2** maintain dominant $^3\pi$-π^* character with less attributes of ICT character [42, 51, 52]. Quantum chemical calculations are expected to have a more accurate description of the excited-state electronic structures, which is helpful to understand the solvent-dependent excited-state relaxation processes.

B. Quantum chemical calculations

On the basis of DFT and TD-DFT calculations, optimized ground-state geometries and the contour plots of molecular orbitals for complexes **1** and **2** in MeCN are shown in FIG. 2 and 3; their corresponding simulated energies, oscillator strengths and main orbital contributions of vertical transitions, including the ^{1}MLCT transitions, are depicted in Tables II and III.

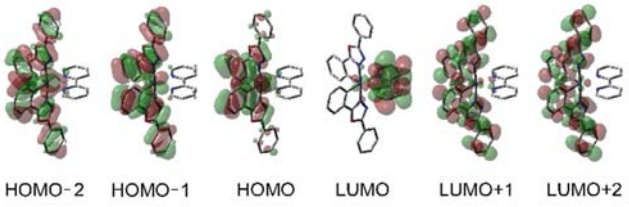

FIG. 2 TDDFT calculated MOs contour plots of complex **1** in MeCN associated with ^{1}MLCT transitions.

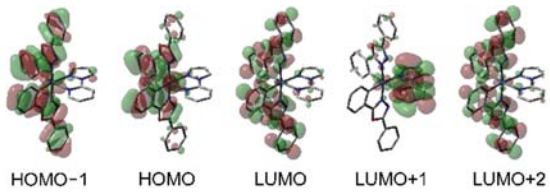

FIG. 3 TDDFT calculated MOs contour plots of complex **2** in MeCN associated with ^{1}MLCT transitions.

In MeCN as solvent, all frontier orbitals exhibit localizations and distributions on segments of the molecules, as shown in FIG. 2 and 3. For both complexes **1** and **2**, the HOMO orbitals are localized on d orbitals of iridium ions and π orbitals of the dph-oxd ligands. The LUMO of complex **1** is delocalized over the bpy ligand, and the LUMO of complex **2** is delocalized over the dph-oxd ligand. For complex **2**, the localization of LUMO on dph-oxd rather on pzpy should be caused by the electron-rich characteristic (leading to higher energy levels of unoccupied molecular orbitals) of the pzpy ligand. Accordingly, the absorption bands between 360 and 450 nm, as shown in FIG. 1, are mainly attributed to the contributions from Ir→ligands (^{1}MLCT, d→π^*) and ligand-centered (^{1}LC, π→π^*) transitions. More specifically, the ^{1}MLCT/^{1}LC transitions (Ir→dph-oxd/dph-oxd-centered, S_0→S_2 for **1** and S_0→S_1 for **2**) have major contribution to the 400 nm (E_{photon}=3.10 eV) absorption for both complexes **1** and **2**. For complex **1**, the ^{1}MLCT/^{1}LLCT transition (Ir→bpy/dph-oxd→bpy, S_0→S_1), as shown in Table II, exists at a relatively low energy (2.87 eV) and has considerable contribution to the 400 nm absorption. Nevertheless, for complex **2**, the ^{1}MLCT/^{1}LLCT (Ir→pzpy/dph-oxd→pzpy, S_0→S_2) transition, as shown in Table III, has an excessive excitation energy (3.31 eV) that is larger than 400 nm absorption. Therefore, for complex **2**, the ^{1}MLCT/^{1}LC transition dominates the 400 nm absorption. Similarly, in THF and $CHCl_3$, the S_0→S_1 transition of complex **1** exhibits the ^{1}MLCT/^{1}LLCT (Ir→bpy/dph-oxd→bpy) character with relatively low excitation energies (∼2.8 eV), whereas in complex **2**,

DOI:10.1063/1674-0068/30/cjcp1703058

TABLE II TDDFT calculated electronic transition properties of complex **1** in MeCN (E_t: transition energy, f: oscillator strength).

	E_t/eV (nm)	f	Main orbital contribution
$S_0 \rightarrow S_1$	2.866 (432.6)	0.0011	HOMO→LUMO
$S_0 \rightarrow S_2$	3.227 (384.2)	0.2227	HOMO→LUMO+1
$S_0 \rightarrow S_3$	3.272 (378.9)	0.0341	HOMO−1→LUMO
$S_0 \rightarrow S_4$	3.351 (367.0)	0.0003	HOMO−2→LUMO
$S_0 \rightarrow S_5$	3.364 (368.5)	0.0109	HOMO→LUMO+2

TABLE III TDDFT calculated electronic transition properties of complex **2** in MeCN.

	E_t/eV (nm)	f	Main orbital contribution
$S_0 \rightarrow S_1$	3.242 (382.4)	0.2267	HOMO→LUMO
$S_0 \rightarrow S_2$	3.308 (374.8)	0.0036	HOMO→LUMO+1
$S_0 \rightarrow S_3$	3.380 (366.8)	0.0081	HOMO→LUMO+2
$S_0 \rightarrow S_4$	3.639 (340.7)	0.0634	HOMO−1→LUMO
$S_0 \rightarrow S_5$	3.698 (335.3)	0.0284	HOMO−1→LUMO+2

the ^{1}MLCT/^{1}LLCT transitions show higher excitation energies (∼3.2 eV) and the ^{1}MLCT/^{1}LC (Ir→dph-oxd/dph-oxd-centered) transitions show the lowest excitation energies.

Furthermore, from our previous calculation results on triplet manifolds [10], for complex **1**, the T3 (^{3}MLCT/^{3}LLCT, Ir→bpy and dph-oxd→bpy) and T1 (^{3}LC/^{3}MLCT, dph-oxd-centered and Ir→dph-oxd) states have close-lying energy levels (2.70 *vs.* 2.54 eV). For complex **2**, the ^{3}MLCT/^{3}LLCT state (T7) lies much higher in energy than T1 (3.11 *vs.* 2.55 eV) and the lower triplet states all have dominant ^{3}LC/^{3}MLCT character.

Therefore, both complexes **1** and **2** could be selectively excited to the ^{1}MLCT states upon the 400 nm excitation. Due to their similar structures but different ancillary ligands, the low-lying singlet and triplet states of complex **1** have MLCT/LLCT character with remarkable changes of electric dipole moments; however, for complex **2**, only the MLCT transition could be induced, forming partial ICT states along with less changes of electric dipole moments. The noteworthy ICT differences between complexes **1** and **2** could be further determined by the following time-resolved transient absorption measurements, where the solvent-dependent excited-state dynamics for both complexes **1** and **2** were explored.

C. Femtosecond transient absorption spectra

The femtosecond transient absorption spectra of complexes **1** and **2** in MeCN upon 400 nm excitation and the transient absorption kinetics curves are depicted in FIG. 4. It is found that, the board excited-state absorption (ESA) bands are generated in initial several hundred femtoseconds. In a few picoseconds, the ESA bands decay gradually. Then, they become stable in the entire delay time down to 1 ns, indicating a long-lived spectral species left. According to steady-state spectra of complexes **1** and **2**, the ground-state absorptions are mainly below 420 nm. Thus, there is negligible spectral overlapping of ground-state bleaching with the ESA spectral range in the observed transient absorption spectra. Furthermore, due to the heavy atom effect, the strong SOC results in an ultrafast ISC within the time scale of several hundred femtoseconds after the Franck-Condon excitation, leading to an accumulation of excited electrons on the triplet manifolds [30, 41]. According to the transition selection rules, the transitions between the triplet and the singlet excited-states are highly forbidden. Therefore, there is no stimulated emission in the observed transient absorption spectra.

In order to explore the relaxation dynamic processes of excited states, global analysis was used to obtain the best fits of the time-resolved absorption spectra with a sequential model, as shown in Scheme 2. For complex **1** in MeCN, three lifetimes are required to adequately fit the evolution dynamics data. As depicted in FIG. 4(c), the rapid, slow and long-lived dynamic processes with the time constants of 0.7 ps, 20 ps, and >1 ns are obtained from the iterative calculations, respectively. The absolute amplitude of each dynamic curve represents the time-dependent concentration evolution of three components, respectively [53]. The first rapid process about 0.7 ps is assigned to the ultrafast ISC and the inertial part of solvent response [54–58], leading to the formation of ^{3}MLCT state [41, 58]. Simultaneously, the energy of the molecular system dissipates to the solvent environment by the inertial part of solvent response, further lowering the energy of the ^{3}MLCT state [40]. The slow component about 20 ps is attributed to the intramolecular vibrational relaxation (IVR) and internal conversion (IC) of the triplet manifold, including the geometrical relaxation of ligands and aromatic nucleus [41, 59], together with the diffusive part of solvation response [55], resulting in the formation of the lowest triplet state. The slowest component with a time constant of >1 ns is attributed to the relaxation from the lowest emissive triplet state to the ground state by radiative and non-radiative relaxations. Actually, the lifetime should be around ∼1 μs, which is further measured by the nanosecond transient absorption spectroscopy in the condition of air-saturated solution. As shown in FIG. 5, the nanosecond probe transient spectra taken at the delay of 10−800 ns for complex **2** in MeCN were plotted with the phosphorescence emission curve and the femtosecond transient absorption spectrum taken at 1 ns. Considering the emission curve, the 100 ns time scale transient absorption spectral profiles are spectrally identical with those taken at 1 ns. The nanosecond transient absorption decay monoexponentially back to the ground state, and no intermediate state is observed. Thus, these spectral decay

DOI:10.1063/1674-0068/30/cjcp1703058

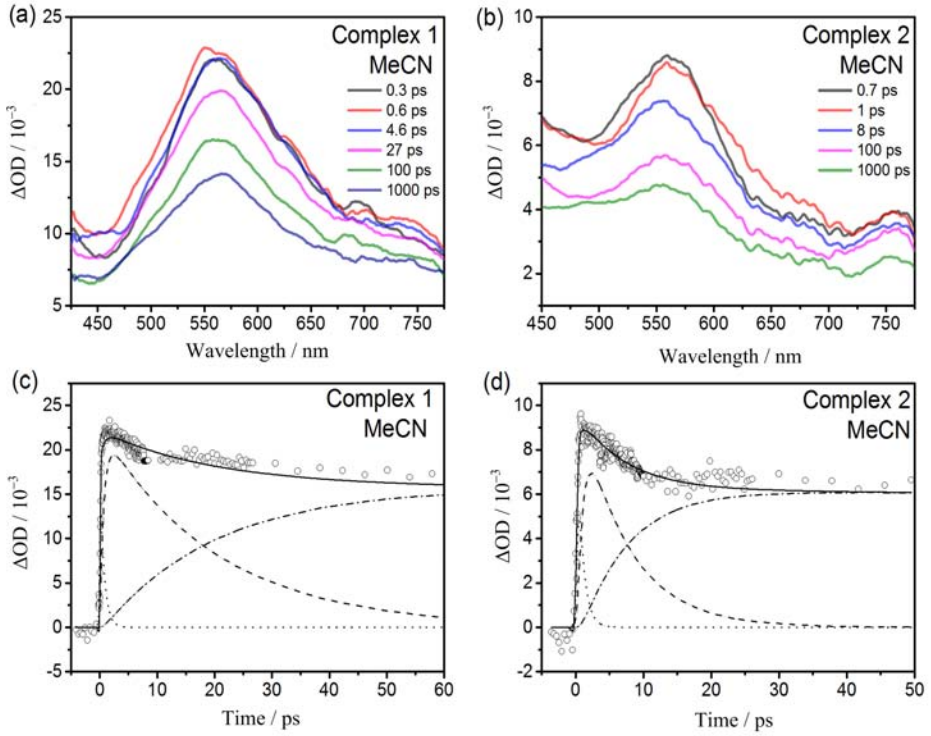

FIG. 4 Femtosecond transient absorption spectra of (a) complex **1** and (b) complex **2** in MeCN following the excitation at 400 nm. Transient absorption kinetics curves of (c) complex **1** and (d) complex **2** probed at 570 nm. The dotted, dashed and dashed-dotted lines obtained from the best fitting, represent the rapid, slow, and the long-lived components, respectively. The solid curves are the best-fitted data as indicated for showing the quality of global fitting results.

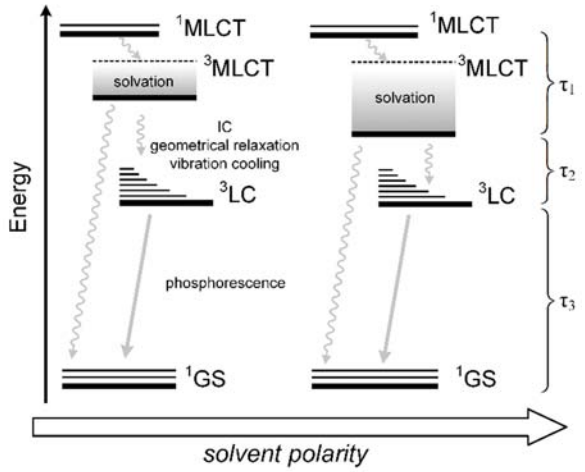

Scheme 2 Relaxation pathway of cationic iridium(III) complexes **1** and **2**. IC=internal conversion, ISC=intersystem crossing, GS=ground state, MLCT=metal-to-ligand charge-transfer state, LC=ligand-centered state.

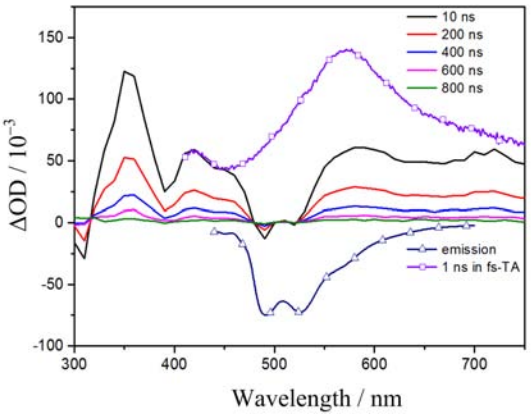

FIG. 5 Femtosecond and nanosecond transient absorption spectra of complex **2** in MeCN taken at the delay of 1 and 10, 200, 400, 600, 800 ns, along with the phosphorescence emission spectral profile.

indicates the lifetime of the lowest triplet state, while the fitting results of complexes **1** and **2** were shown in Table IV.

For complex **2** in MeCN, as depicted in FIG. 4 (b) and (d), three lifetimes of 0.8 ps, 7 ps, and >1 ns are obtained from the global fitting. Similarly, these components are assigned to the solvent stabilized ^{3}MLCT state, vibrational cooling and geometrical relaxation within the triplet manifold, and long-lived ^{3}LC, respectively.

Generally, the excited state dynamics, especially for molecules with ICT character, are intensely affected by the nature of solvent [60]. Besides the strong polar

DOI:10.1063/1674-0068/30/cjcp1703058

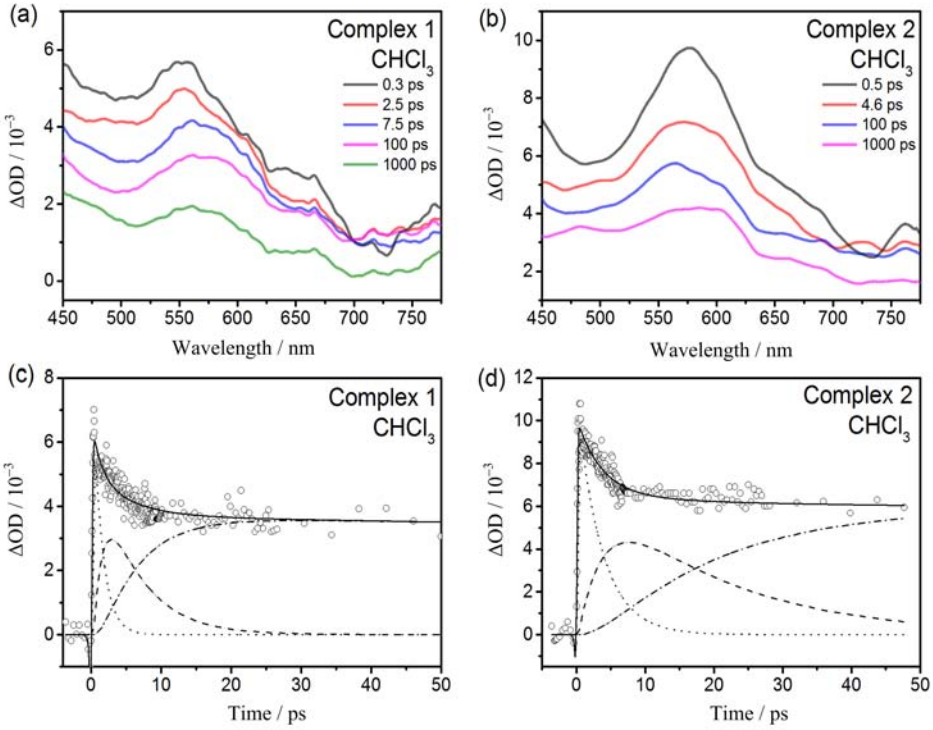

FIG. 6 Femtosecond transient absorption spectra of (a) complex **1** and (b) complex **2** in $CHCl_3$ following the excitation at 400 nm. Transient absorption kinetics curves of (c) complex **1** and (d) complex **2** probed at 570 nm, the dotted, dashed and dashed-dotted lines obtained from the best fitting, represent the rapid, slow, and the long-lived components, respectively; the solid curves are the best-fitted data as indicated for showing the quality of global fitting dotted.

solvent MeCN (ε=35.94), we further investigated the excited-state relaxations of complexes **1** and **2** by femtosecond transient absorption spectroscopy in less polar solvent $CHCl_3$ (ε=4.81) and THF (ε=7.58) [44]. As shown in FIG. 6, similarly to the spectral evolutions in MeCN, the broad ESA bands form rapidly after the optical excitations, followed by a decay in the time scale of several picoseconds till a long-lived species remained within the measuring time range. Through the global analysis, three components corresponding to the rapid, slow, and long-lived dynamic processes, respectively, are also obtained. All fitting results are listed in Table IV.

The solvation mainly affects the rapid decay component within ∼1 ps, which includes the ISC and the generation of solvent stabilized ICT states [59, 61]. For complex **1**, the solvent-dependent time of the rapid process increases from 0.7 ps in MeCN, and 1.0 ps in THF to 1.4 ps in $CHCl_3$, along with the decrease of the solvent polarity. The same tendency is observed for complex **2** as well. In a polar solvent, such as MeCN, the ^{3}MLCT is highly stabilized by the fast solvation because of the strong dipole-dipole interaction, while the potential energy surface lowers and lies at an energy level close to the emissive ^{3}LC state [40]. According to the energy gap law, such solvation-induced stabilization results in a decrease of the triplet-state lifetime and the luminescence quantum yield [60]. In contrast, in less polar solvents, such as THF and $CHCl_3$, the ^{3}MLCT states are destabilized with a higher energy to ^{3}LC states because of weak solvation, leading to longer-lived emissive triplet states and higher quantum yields.

TABLE IV Solvent-dependent relaxation dynamics parameters for complexes **1** and **2** after 400 nm excitation.

	Solvent	ε^a	$\tau_1{}^b$/ps	$\tau_2{}^b$/ps	$\tau_3{}^b$/ns	$\tau_4{}^c$/ns
1	MeCN	35.94	0.7±0.10	20±0.5	>1	230±10
2			0.8±0.06	7±0.8	>1	260±10
1	THF	7.58	1.0±0.10	5±0.8	>1	450±10
2			1.2±0.06	13±0.5	>1	300±15
1	$CHCl_3$	4.81	1.4±0.06	6±0.8	>1	600±10
2			3.6±0.06	18±0.5	>1	650±10

[a] ε is the dielectric constant of the solven [44].
[b] Dynamics parameters in femtosecond transient absorption obtained from the global analysis.
[c] The lifetime of the ESA measured by nanosecond transient absorption at 600 nm in air-saturated solution.

Furthermore, complexes **1** and **2** show a small discrepancy in solvent-dependent excited-state dynamics due to their different excited-state ICT features. As shown in the steady-state spectra and quantum chemical calculations, the lowest excited-states of complexes **1** and **2** both contain dominant π-π^* characteristics. However, considerable MLCT/LLCT transitions

DOI:10.1063/1674-0068/30/cjcp1703058

of complex **1** can be induced by the low-energy excitation at 400 nm. In femtosecond transient absorption spectra, the lifetimes (τ_1) for the formation of solvent stabilized ^{3}MLCT states are relatively shorter for complex **1** than that for complex **2** in the same solvent as shown in Table IV. Because solvent molecules rearrange around the excited molecules according to the charge-density redistribution [40], the solvation process is faster and more drastic for solute molecules containing strong ICT character [60]. As shown in Scheme 2, the $S_0 \rightarrow S_1/S_2$ (^{1}MLCT/^{1}LLCT) transitions of complex **1** can be efficiently excited with 400 nm excitation (E_{photon}=3.10 eV), which facilitates the population of T_3 (^{3}MLCT/^{3}LLCT) through the rapid ISC. During this process, the charge density of complex **1** is highly separated, and molecules on ICT states are solvated simultaneously till the charge recombination happens. For complex **2**, after the $S_0 \rightarrow S_1$ (^{1}MLCT) excitation at 400 nm, excited molecules undergo ISC quickly and accumulate on triplet manifolds. Due to the excessive energy level of ^{3}LLCT/^{3}MLCT (T_7) state, excited complex **2** at ^{1}MLCT state has greater odds to straightly relax to lower-lying triplet states with weak ICT character, leading to weaker and slower solvation relative to that of complex **1**. The first component in relaxation process is associated with the solute ICT property and solvent polarity. The second component includes the IC from the ^{3}MLCT state to the lowest emissive ^{3}LC state, together with an electron-hole recombination in excited states along with a solvation process of an IVR of the solute molecules about ∼10 ps. Specifically, the octahedral coordination complexes may also have multiple rotational and vibrational degrees of freedom since complexes **1** and **2** have different ancillary ligands, which can not be identified from observed results.

IV. CONCLUSION

In this work, we have investigated two phosphorescent cationic iridium(III) complexes [Ir(dph-oxd)$_2$(bpy)]PF$_6$ (**1**) and [Ir(dph-oxd)$_2$(pzpy)]PF$_6$ (**2**) to reveal their solvent-dependent photoluminescence properties and excited-state dynamics. Based on the steady-state spectra and quantum chemical calculations, both complexes have remarkable MLCT character in their low-energy transitions, while the LLCT transition in complex **1** is easier to be formed than that in complex **2** upon 400 nm excitation. Through the transient absorption spectroscopy measurements with the excitation of ^{1}MLCT state, we have figured out the formation (τ=0.7−3 ps) of solvent stabilized ^{3}MLCT via ISC, which is affected by the solvent polarity. In addition, the vibrational cooling/geometry relaxation (τ=5−20 ps) and long-lived phosphorescent emission processes (τ=∼1 μs) were identified.

In summary, for spin-mixed phosphorescent iridium(III) complexes, the solvation induces a prompt generation of solvent stabilized ^{3}MLCT states and lowers the potential energy surfaces, which indeed influence the phosphorescence quantum yield. The present work provides a better insight of solvent dependent emission properties and excited state relaxation dynamics of iridium(III) complexes.

V. ACKNOWLEDGMENTS

This work is supported by the National Basic Research Program of China (No.2013CB834604), the National Natural Foundation of China (No.21673252, No.21333012, No.21373232, and No.51403240) and the Strategic Priority Research Program of the Chinese Academy of Sciences (No.XDB12020200).

[1] M. A. Baldo, M. E. Thompson, and S. R. Forrest, Nature **403**, 750 (2000).
[2] X. L. Yang, G. J. Zhou, and W. Y. Wong, Chem. Soc. Rev. **44**, 8484 (2015).
[3] C. Adachi, M. A. Baldo, M. E. Thompson, and S. R. Forrest, J. Appl. Phys. **90**, 5048 (2001).
[4] A. Monguzzi, R. Tubino, and F. Meinardi, Phys. Rev. B **77**, 155122 (2008).
[5] T. N. Singh-Rachford and F. N. Castellano, Coord. Chem. Rev. **254**, 2560 (2010).
[6] W. Y. Wong and C. L. Ho, Acc. Chem. Res. **43**, 1246 (2010).
[7] S. Y. Takizawa, R. Aboshi, and S. Murata, Photochem. Photobiol. Sci. **10**, 895 (2011).
[8] J. I. Goldsmith, W. R. Hudson, M. S. Lowry, T. H. Anderson, and S. Bernhard, J. Am. Chem. Soc. **127**, 7502 (2005).
[9] L. He, D. X. Ma, L. Duan, Y. G. Wei, J. Qiao, D. Q. Zhang, G. F. Dong, L. D. Wang, and Y. Qiu, Inorg. Chem. **51**, 4502 (2012).
[10] Z. Wang, L. He, L. Duan, J. Yan, R. R. Tang, C. Y. Pan, and X. Z. Song, Dalton Trans. **44**, 15914 (2015).
[11] Y. M. You and S. Y. Park, Dalton Trans. 1267 (2009).
[12] Y. M. You and W. Nam, Chem. Soc. Rev. **41**, 7061 (2012).
[13] E. M. Kober and T. J. Meyer, Inorg. Chem. **21**, 3967 (1982).
[14] L. Flamigni, A. Barbieri, C. Sabatini, B. Ventura, and F. Barigelletti, *Photochemistry and Photophysics of Coordination Compounds: Iridium*, V. Balzani and S. Campagna Eds., Berlin, Heidelberg: Springer, 143 (2007).
[15] B. Ma, P. I. Djurovich, S. Garon, B. Alleyne, and M. E. Thompson, Adv. Funct. Mater. **16**, 2438 (2006).
[16] M. Pfeiffer, S. R. Forrest, K. Leo, and M. E. Thompson, Adv. Mater. **14**, 1633 (2002).
[17] J. Li, P. I. Djurovich, B. D. Alleyne, M. Yousufuddin, N. N. Ho, J. C. Thomas, J. C. Peters, R. Bau, and M. E. Thompson, Inorg. Chem. **44**, 1713 (2005).
[18] G. J. Hedley, A. Ruseckas, and I. D. W. Samuel, Chem. Phys. Lett. **450**, 292 (2008).
[19] G. J. Hedley, A. Ruseckas, and I. D. W. Samuel, J. Phys. Chem. A **113**, 2 (2009).

DOI:10.1063/1674-0068/30/cjcp1703058

[20] G. J. Hedley, A. Ruseckas, and I. D. W. Samuel, J. Phys. Chem. A **114**, 8961 (2010).
[21] C. H. Yang, Y. M. Cheng, Y. Chi, C. J. Hsu, F. C. Fang, K. T. Wong, P. T. Chou, C. H. Chang, M. H. Tsai, and C. C. Wu, Angew. Chem. Int. Ed. **46**, 2418 (2007).
[22] D. Escudero and W. Thiel, Inorg. Chem. **53**, 11015 (2014).
[23] P. T. Chou, Y. I. Liu, H. W. Liu, and W. S. Yu, J. Am. Chem. Soc. **123**, 12119 (2001).
[24] J. Seo, S. Kim, and S. Y. Park, J. Am. Chem. Soc. **126**, 11154 (2004).
[25] W. Dang, J. J. Bai, L. S. Zhang, and Y. X. Weng, Chin. J. Chem. Phys. **29**, 147 (2016).
[26] J. K. McCusker, Acc. Chem. Res. **36**, 876 (2003).
[27] S. A. Kovalenko, R. Schanz, H. Hennig, and N. P. Ernsting, J. Chem. Phys. **115**, 3256 (2001).
[28] L. L. Jiang, W. L. Liu, Y. F. Song, X. He, Y. Wang, H. L. Wu, and Y. Q. Yang, Chin. J. Chem. Phys. **25**, 577 (2012).
[29] S. Murphy, L. B. Huang, and P. V. Kamat, J. Phys. Chem. C **115**, 22761 (2011).
[30] G. B. Shaw, C. D. Grant, H. Shirota, E. W. Jr. Castner, G. J. Meyer, and L. X. Chen, J. Am. Chem. Soc. **129**, 2147 (2007).
[31] L. Q. Song, J. Feng, X. S. Wang, J. H. Yu, Y. J. Hou, P. H. Xie, B. W. Zhang, J. F. Xiang, X. C. Ai, and J. P. Zhang, Inorg. Chem. **42**, 3393 (2003).
[32] C. S. Ma, C. T. L. Chan, W. M. Kwok, and C. M. Che, Chem. Sci. **3**, 1883 (2012).
[33] J. H. Hu, Q. Zhang, and Y. Luo, J. Phys. Chem. Lett. **7**, 3908 (2016).
[34] W. Y. Wong and C. L. Ho, Coord. Chem. Rev. **253**, 1709 (2009).
[35] M. J. Frisch, G. W. Trucks, H. B. Schlegel, G. E. Scuseria, M. A. Robb, J. R. Cheeseman, G. Scalmani, V. Barone, B. Mennucci, G. A. Petersson, H. Nakatsuji, M. Caricato, X. Li, H. P. Hratchian, A. F. Izmaylov, J. Bloino, G. Zheng, J. L. Sonnenberg, M. Hada, M. Ehara, K. Toyota, R. Fukuda, J. Hasegawa, M. Ishida, T. Nakajima, Y. Honda, O. Kitao, H. Nakai, T. Vreven, J. A. Montgomery, J. E. Peralta, F. Ogliaro, M. Bearpark, J. J. Heyd, E. Brothers, K. N. Kudin, V. N. Staroverov, R. Kobayashi, J. Normand, K. Raghavachari, A. Rendell, J. C. Burant, S. S. Iyengar, J. Tomasi, M. Cossi, N. Rega, J. M. Millam, M. Klene, J. E. Knox, J. B. Cross, V. Bakken, C. Adamo, J. Jaramillo, R. Gomperts, Stratmann, O. Yazyev, A. J. Austin, R. Cammi, C. Pomelli, J. W. Ochterski, R. L. Martin, K. Morokuma, V. G. Zakrzewski, G. A. Voth, P. Salvador, J. J. Dannenberg, S. Dapprich, A. D. Daniels, Ö. Farkas, J. B. Foresman, J. V. Ortiz, J. Cioslowski, and D. J. Fox, *Gaussian 09 (Revision A.02)*, Wallingford CT: Gaussian Inc., (2009).
[36] Y. Li, M. Zhou, Y. L. Niu, Q. J. Guo, and A. D. Xia, J. Chem. Phys. **143**, 034309 (2015).
[37] M. Zhou, S. Vdović, S. Long, M. Z. Zhu, L. Y. Yan, Y. Y. Wang, Y. L. Niu, X. F. Wang, Q. J. Guo, R. C. Jin, and A. D. Xia, J. Phys. Chem. A **117**, 10294 (2013).
[38] I. H. M. van Stokkum, D. S. Larsen, and R. van Grondelle, Biochim. Biophys. Acta **1657**, 82 (2004).
[39] J. J. Snellenburg, S. P. Laptenok, R. Seger, K. M. Mullen, and I. H. M. van Stokkum, J. Stat. Soft. **49**, 1 (2012).
[40] M. Zhou, Z. Lei, Q. J. Guo, Q. M. Wang, and A. D. Xia, J. Phys. Chem. C **119**, 14980 (2015).
[41] C. Y. Chen, H. R. Tsai, K. Y. Lu, H. H. Yao, Y. H. O. Yang, C. H. Cheng, and I. C. Chen, J. Chin. Chem. Soc. **60**, 965 (2013).
[42] M. G. Colombo, T. C. Brunold, T. Riedener, H. U. Guedel, M. Fortsch, and H. B. Buergi, Inorg. Chem. **33**, 545 (1994).
[43] S. Sprouse, K. A. King, P. J. Spellane, and R. J. Watts, J. Am. Chem. Soc. **106**, 6647 (1984).
[44] M. L. Horng, J. A. Gardecki, A. Papazyan, and M. Maroncelli, J. Phys. Chem. **99**, 17311 (1995).
[45] M. L. Jia, X. N. Ma, L. Y. Yan, H. F. Wang, Q. J. Guo, X. F. Wang, Y. Y. Wang, X. W. Zhan, and A. D. Xia, J. Phys. Chem. A **114**, 7345 (2010).
[46] G. G. Shan, H. B. Li, H. T. Cao, D. X. Zhu, P. Li, Z. M. Su, and Y. Liao, Chem. Commun. **48**, 2000 (2012).
[47] T. F. Mastropietro, Y. J. Yadav, E. I. Szerb, A. M. Talarico, M. Ghedini, and A. Crispini, Dalton Trans. **41**, 8899 (2012).
[48] H. B. Sun, S. J. Liu, W. P. Lin, K. Y. Zhang, W. Lv, X. Huang, F. W. Huo, H. R. Yang, G. Jenkins, Q. Zhao, and W. Huang, Nat. Commun. **5**, 3601 (2014).
[49] X. Q. Zhang, Z. G. Chi, Y. Zhang, S. W. Liu, and J. R. Xu, J. Mater. Chem. C **1**, 3376 (2013).
[50] Y. Han, H. T. Cao, H. Z. Sun, Y. Wu, G. G. Shan, Z. M. Su, X. G. Hou, and Y. Liao, J. Mater. Chem. C **2**, 7648 (2014).
[51] H. J. Bolink, L. Cappelli, S. Cheylan, E. Coronado, R. D. Costa, N. Lardiés, M. K. Nazeeruddin, and E. Ortí, J. Mater. Chem. **17**, 5032 (2007).
[52] A. B. Tamayo, S. Garon, T. Sajoto, P. I. Djurovich, I. M. Tsyba, R. Bau, and M. E. Thompson, Inorg. Chem. **44**, 8723 (2005).
[53] Y. P. Wang, S. Zhang, S. M. Sun, K. Liu, and B. Zhang, Chin. J. Chem. Phys. **26**, 651 (2013).
[54] J. R. Huang, O. Buyukcakir, M. W. Mara, A. Coskun, N. M. Dimitrijevic, G. Barin, O. Kokhan, A. B. Stickrath, R. Ruppert, D. M. Tiede, J. F. Stoddart, J. P. Sauvage, and L. X. Chen, Angew. Chem. Int. Ed. **51**, 12711 (2012).
[55] M. Zhou, S. R. Long, X. K. Wan, Y. Li, Y. L. Niu, Q. J. Guo, Q. M. Wang, and A. D. Xia, Phys. Chem. Chem. Phys. **16**, 18288 (2014).
[56] X. X. Zhang, M. Liang, N. P. Ernsting, and M. Maroncelli, J. Phys. Chem. B **117**, 4291 (2013).
[57] V. A. Lenchenkov, C. X. She, and T. Q. Lian, J. Phys. Chem. B **108**, 16194 (2004).
[58] G. Ramakrishna, T. Goodson III, J. E. Rogers-Haley, T. M. Cooper, D. G. McLean, and A. Urbas, J. Phys. Chem. C **113**, 1060 (2009).
[59] Y. J. Sun, Y. Liu, and C. Turro, J. Am. Chem. Soc. **132**, 5594 (2010).
[60] Y. J. Sun and C. Turro, Inorg. Chem. **49**, 5025 (2010).
[61] S. Q. Yang and K. L. Han, J. Phys. Chem. A **120**, 4961 (2016).

DOI:10.1063/1674-0068/30/cjcp1703058